scientific reports

Check for updates

OPEN

Forensic gemmological investigation based on optical and crystal-chemical changes in topaz from Ouro Preto and Caraí, Brazil, induced by heat treatment

Jana Fridrichová[1]✉, Peter Bačík[1], Olena Rybnikova[1], Ján Štubňa[3], Daniel Furka[4], Samuel Furka[4], Jan Cempírek[2], Radek Škoda[2] & Tomáš Vaculovič[5,6]

Topaz is frequently subjected to heat treatment and irradiation to enhance colour, particularly to produce the market's most preferred salmon pink and sky blue varieties. However, an insufficient description of these processes can lead to fraudulent practices. This experimental and forensic mineralogical and gemmological study investigates eighteen heat-treated topaz samples from Ouro Preto (OP) and Caraí (CA), Brazil, using electron microanalysis, LA-ICP-MS, Raman, and optical absorption spectroscopy before and after heat treatment at various temperatures. The most significant optical changes were observed at 300 °C when the CA sample lost its colour from sky blue to colourless, while OP samples retained their imperial orange colour up to 500 °C before transitioning to pink at 700 °C. Chemically, the CA samples are rich in F (> 1.8 *apfu*) with low trace element concentration (Fe ≤ 125 ppm, Ge ≤ 153 ppm), falling to the pegmatite and greisen field of topaz origin. The OP samples contain less F (1.4–1.5 *apfu*) but higher trace element contents (Cr up to 204 ppm, Ti up to 115 ppm, Fe, Mn, Ge < 64 ppm), consistent with a hydrothermal origin. Raman spectra show no significant inter-sample variation, but their luminescence spectra feature strong differences: Mn acts as the luminophore in CA samples, while Cr^{3+} centers dominate in OP samples. The optical absorption spectra reveal distinct thermal responses. The OP samples heated to temperatures ≥ 500 °C developed new absorption bands at 530–532 nm, consequently resulting in a visible pink colour. On the other hand, the CA spectra exhibit strong absorption in the NIR region; the unheated sample has a broad absorption band at 634 nm, responsible for the sky-blue colour of topaz. Heating ≥ 300 °C eliminates the transmission window in the blue to cyan regions, removing blue colouration. These thermal-optical signatures serve as indicators of heat treatment in topaz declared from these two localities. Moreover, the combination of spectroscopic methods, which we successfully applied in recognizing heat treatment on the studied samples, provides a systematic approach for identifying treatment in topaz and potentially other gemstones.

Keywords Topaz, Chemical composition, Heat treatment, Optical absorption spectroscopy, Raman spectroscopy, Gemmology

[1]Department of Mineralogy, Petrology and Economic Geology, Faculty of Natural Sciences, Comenius University in Bratislava, Ilkovičova 6, Bratislava 842 15, Slovakia. [2]Department of Geological Sciences, Faculty of Science, Masaryk University, Kotlářská 2, Brno 611 37, Czech Republic. [3]Gemmological Laboratory, Department of Geography Geoinformatics and Regional Development, Faculty of Natural Sciences and Informatics, Constantine the Philosopher University in Nitra, Nábrežie mládeže 91, Nitra 94901, Slovakia. [4]Department of Physical and Theoretical Chemistry, Faculty of Natural Sciences, Comenius University, Ilkovičova 6, Bratislava 842 15, Slovakia. [5]Department of Chemistry, Faculty of Science, Masaryk University, Kamenice 5, Brno 625 00, Czech Republic. [6]Institute of Laboratory Research on Geomaterials, Faculty of Natural Science, Comenius University in Bratislava, Mlynska dolina, Ilkovicova 6, Bratislava 4 842 15, Slovakia. ✉email: jana.fridrichova@uniba.sk

Topaz, $Al_2SiO_4(F, OH)_2$, is one of the most preferred gemstones. Its value depends on colour, clarity, weight, cut, and rarity. Coloured varieties are much more precious than colourless ones. Intensive, vivid colours are more desirable than pale ones.

Topaz is the F/OH-bearing silicate, mainly found as an accessory mineral in F-rich granitic rocks associated with pneumatolithic/hydrothermal processes and in ultrahigh-pressure rocks[1–5]. Topaz is a stable phase above 12 GPa and 1100°C[4,6–8]. The crystal structure of natural topaz was independently solved by[9,10] and reinvestigated by several authors[5,11–14]. Topaz is an orthosilicate, and its structure consists of chains of edge-sharing $Al(O, F,OH)_6$-octahedra connected by isolated SiO_4-tetrahedra. The proton forming the OH group with the O4 atom is located in a cavity adjacent to the $Al(O, F, OH)_6$-octahedra. The crystal chemistry and physical properties of topaz have been extensively investigated along the solid solution $Al_2SiO_4F_2$-$Al_2SiO_4(OH)_2$ by means of optical microscopy, IR spectroscopy, and X-ray diffraction[15–31].

Pure topaz is colourless; however, several coloured varieties of topaz are known. Natural blue topaz is rare and expensive; some topaz samples from Brazil and Zimbabwe show a light blue colour[32]. Intensive blue topaz colour can be gained by irradiation, subsequently followed by heating[33–35]. The blue topaz of various colour intensities appeared at the gemstone market under the trade names "London blue", "Swiss blue", and "Sky blue". Pink topaz is extremely rare and very valuable, usually marketed as "imperial topaz"; it is frequently obtained by heat treatment from the orange material[36]. Until today, the techniques to enhance gemstone colour have become more sophisticated. Nowadays, with the advancement of science and technology, new opportunities for gemstone enhancement and the synthesis of gemstones have been developed. Many retailers without the necessary education in the field offer a wide range of gemstones without a thorough knowledge of their origin, and they often inadvertently deceive the final consumer.

This research was developed to provide information on topaz heat treatment to specialists in the field, as well as gem sellers and consumers. The aim of this study is to diminish the risk of fraud and to improve consumer awareness by characterizing the heat treatment process step by step under precisely defined conditions. Its main purpose is to evaluate information about the gemstones provided by the retailer to protect consumers.

Experimental and analytical methods

We studied crystal-chemical and gemmological properties of coloured topaz from Brazil. The authenticity of imperial topaz from Ouro Preto (sample OP) with its typical orange colour and light blue topaz from Caraí (sample CA) was investigated. We compared unheated and heated samples from both localities at various temperatures based on their optical proportions and chemical composition. We determined the relationship between the main and trace element contents and the extent of substitutions. Topaz samples were subjected to varying temperatures and then analysed by multiple analytical methods to characterize their properties using crystal-chemical and spectroscopic investigation. The topaz chemical composition was determined by electron microprobe (EMPA) and Laser Ablation Inductively Coupled Plasma Mass Spectrometry (LA-ICP-MS), possible structural changes by Raman spectroscopy, and optical changes by optical absorption spectroscopy (OAS).

Eighteen samples of two different topaz varieties, imperial topaz (Ouro Preto - OP) and light blue topaz (Caraí - CA) from Brazil, were studied. The OP samples were declared as not enhanced, whereas the CA samples were irradiated to a sky blue colour according to the seller's statement. Cut slabs from each topaz variety were selected and divided into 9 parts, 2 stones in each part, to be used for different heating procedures. The stones were heated in the muffle furnace at 300 °C (OP 300, CA 300), 400 °C (OP 400, CA 400), 500 °C (OP 500, CA 500), 600 °C (OP 600, CA 600), 700 °C (OP 700, CA 700), 800 °C (OP 800, CA 800), 900 °C (OP 900, CA 900), 1000 °C (OP 1000, CA 1000) and 1100 °C (OP 1100, CA 1100) in the air atmosphere for 12 h. These were subsequently cooled to ambient temperature for 12 h, and macroscopic colour changes and microscopic changes were visually observed and documented. Samples from each part were then prepared for analytical study, and cut stones were embedded in polished sections.

Microscopic examination

Microscopic examination was conducted using Motic GM-171 trinocular microscopes at magnifications ranging from 10× to 50×, employing both darkfield and brightfield illumination techniques to optimize sample visualization and characterization.

Electron microprobe analysis

The chemical composition of topaz crystals was determined using a Cameca SX100 electron microprobe operating in wavelength-dispersive spectroscopy (WDS) mode at the Department of Geological Sciences, Masaryk University. Analytical conditions were set as follows: accelerating voltage of 15 kV, beam current of 20 nA, and beam diameter of 3.0 μm. Calibration was performed using well-characterized mineral and synthetic standards: andradite (Fe *Kα*), spessartine (Mn *Kα*), titanite (Ti *Kα*), wollastonite (Ca *Kα*), andalusite (Si *Kα*), sanidine (K *Kα*), albite (Na *Kα*), Mg_2SiO_4 (Mg *Kα*), Ni_2SiO_4 (Ni *Kα*), $ScVO_4$ (Sc *Kα*), $SrSO_4$ (Sr *Kα*), baryte (Ba *Kα*), chromite (Cr *Kα*), gahnite (Zn *Kα*), topaz (F *Kα*), and vanadinite (V *Kα*, Cl *Kα*). Element detection limits ranged from 150 to 700 ppm across the analytical suite. Crystal-chemical formulae for topaz were calculated on the basis of 3.00 cations per formula unit.

Laser ablation inductively coupled plasma mass spectrometry (LA-ICP-MS)

Trace element analyses were performed using LA-ICP-MS at the Department of Chemistry, Masaryk University, Brno, Czech Republic. The analytical setup consisted of an Analyte G2 + laser ablation system (CETAC Technologies) equipped with a 213 nm Nd: YAG laser, coupled to an Agilent 7900 quadrupole ICP-MS spectrometer (Agilent Technologies, Japan). Samples were positioned within a Helex2 two-volume ablation cell,

and ablated material was transported from the cell using helium carrier gas flows of 0.600 and 0.300 L/min. Argon makeup gas (1.0 L/min) was introduced into the helium flow prior to the ICP-MS interface.

Instrument optimization was performed using NIST SRM 610 glass standard to maximize signal-to-noise ratios while maintaining oxide formation below 0.2% (ThO^+/Th^+) and U^+/Th^+ ratios below 1.1%. Sample ablation parameters were optimized as follows: laser spot diameter of 100 µm, repetition rate of 20 Hz, and laser fluence of 6.0 J/cm^2. Each analytical spot was ablated for 60 s with 30 s intervals between successive spots to allow for washout. Quantitative analysis was performed using NIST SRM 610 glass as the external standard.

Raman spectroscopy

Raman spectroscopic analyses were conducted using a LabRAM-HR Evolution spectrometer system (Horiba Jobin-Yvon) equipped with a Peltier-cooled CCD detector and Olympus BX-41 microscope at the Department of Geological Sciences, Masaryk University. Raman spectra were excited using a 532 nm He-Ne laser, with spectral calibration performed against a silicon wafer reference (520.6 cm^{-1}). Spectra were collected over the range 50–4000 cm^{-1} using a 100× objective, with measurements taken in both parallel and perpendicular orientations relative to the crystallographic Z-axis and laser polarization direction. Data acquisition parameters included 15 s integration time per frame with 2 accumulations to enhance signal-to-noise ratios.

Optical absorption spectroscopy

Optical absorption spectra of faceted gemstone samples were acquired in the visible region (400–750 nm) at room temperature using a GL Gem Spectrometer™ at the Department of Mineralogy, Petrology and Economic Geology, Faculty of Natural Sciences, Comenius University, Bratislava.

Spectral data processing

Both Raman and UV-Vis-NIR spectral data were processed using PeakFit software version 4.1.12 (Systat Software, Inc., San Jose, CA, USA). Spectral deconvolution was performed using Lorentzian peak functions with automated background correction and Savitzky-Golay smoothing algorithms applied to optimize peak resolution and minimize noise.

Results and discussion

Macroscopic and microscopic observations

When observed with the naked eye (Fig. 1), the CA sample exhibited a typical sky-blue colour at room temperature. Its colour intensity decreased from sky blue to colourless already at 300 °C, and remained colourless up to 1100 °C. The clarity rapidly decreased from 700 °C to 1100 °C, accompanied by the formation of cracks and fissures. The OP sample had the orange colour typical for untreated Ouro Preto topaz. The orange colour remained present during heating up to 500 °C; at 600 °C, a pink colour with an orange tint appeared. The gemologically most attractive intense pink colour was obtained at 700 °C; subsequently, its saturation significantly decreased at 800 °C, and from 900 °C up to 1000 °C, we could observe pink colour with orange tint. The temperature of 1100 °C turned the OP sample milky white.

While untreated CA samples were very clean and transparent, OP samples were heavily included, even to the naked eye. However, the increasing temperature had a very positive effect on the clarity of OP samples up to 700 °C. Between 800 °C and 1000 °C, the cracks, fissures, and clouds increased, but clarity remained translucent. It turned opaque at 1100 °C.

The OP samples (Figs. 2 and 3) heated at 300 °C revealed brown-yellow Fe oxide staining on fissures partially converted to red-brown, probably hematite, visible under the optical microscope. Undamaged fluid inclusions were still observed at 400 °C, but at temperatures of 500 °C and up to 700 °C, they were partially dried. Heating to 700 °C caused brown-yellow limonite to convert to red-brown hematite. Fully dried inclusions appeared at temperatures ranging from 800 °C to 1000 1000 °C. The opaque transparency of the OP sample, possibly caused by partial topaz breakdown along fine fractures at 1100 °C, as reported by[37], made observation of the inclusions impossible.

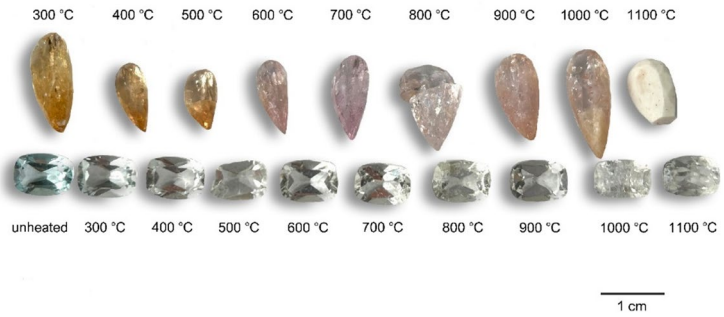

Fig. 1. Macrophotographs of Ouro Preto (OP, upper row) and Caraí (CA, lower row) samples with indication of the heating temperature.

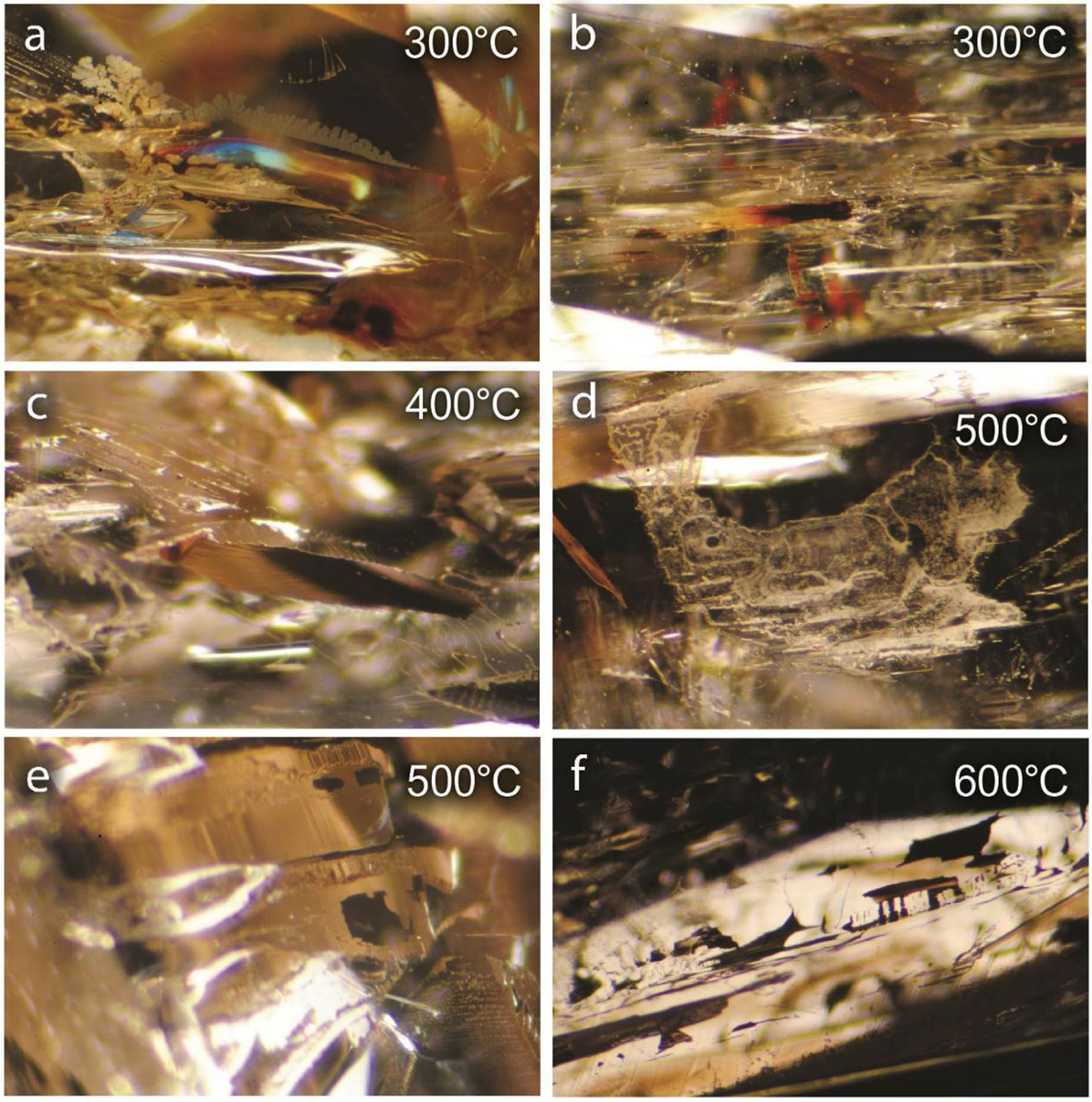

Fig. 2. Microphotographs of inclusions in OP samples heated up to 600 °C: (a) group of small primary fluid inclusions in topaz expanded to relieve pressure (magnification 20x); (b) brownish-yellow Fe oxide partially converted to dark reddish brown (20x); (c) fluid inclusions network (30x); (d) dried fluid inclusions (20x); (e) partially dried fluid inclusions (30x); (f) dried fluid inclusions (20x).

The CA samples showed two-phase fluid inclusions (Figs. 4 and 5) and mineral inclusions, including Fe oxides, were found (Fig. 4b–d). Newly formed orange iron compounds appeared at 300 °C. Subsequently, the fluid inclusions were destroyed, generating fractures along topaz cleavage, and dried at temperatures between 500 °C and 1100 °C. At 1100 °C, the CA samples revealed fully dry inclusions surrounded by fractures with brown staining.

Heat treatment induces significant transformations in topaz, governed by thermal expansion, defect mobility, and phase transitions of entrapped inclusions[38]. Initially, CA topaz exhibited high clarity with well-developed two-phase fluid inclusions, while OP samples showed a higher density of mineral and fluid inclusions, contributing to their greater optical heterogeneity. Upon heating to 300 °C, Fe oxide inclusions in both topaz types began to transform from brownish-yellow to a dark reddish brown phase. In the OP samples, this transformation can be consistent with the topotactic dehydroxylation of FeO(OH) to α-Fe_2O_3, a process thermodynamically favored under dry oxidising conditions, consistent with transformation mechanisms observed in natural goethite-hematite systems[39]. Simultaneously, fluid inclusions in CA samples exhibited progressive decrepitation and volumetric collapse between 500 and 700 °C, indicative of internal overpressure arising from differential thermal expansion and partial volatilisation of entrapped fluids[40].

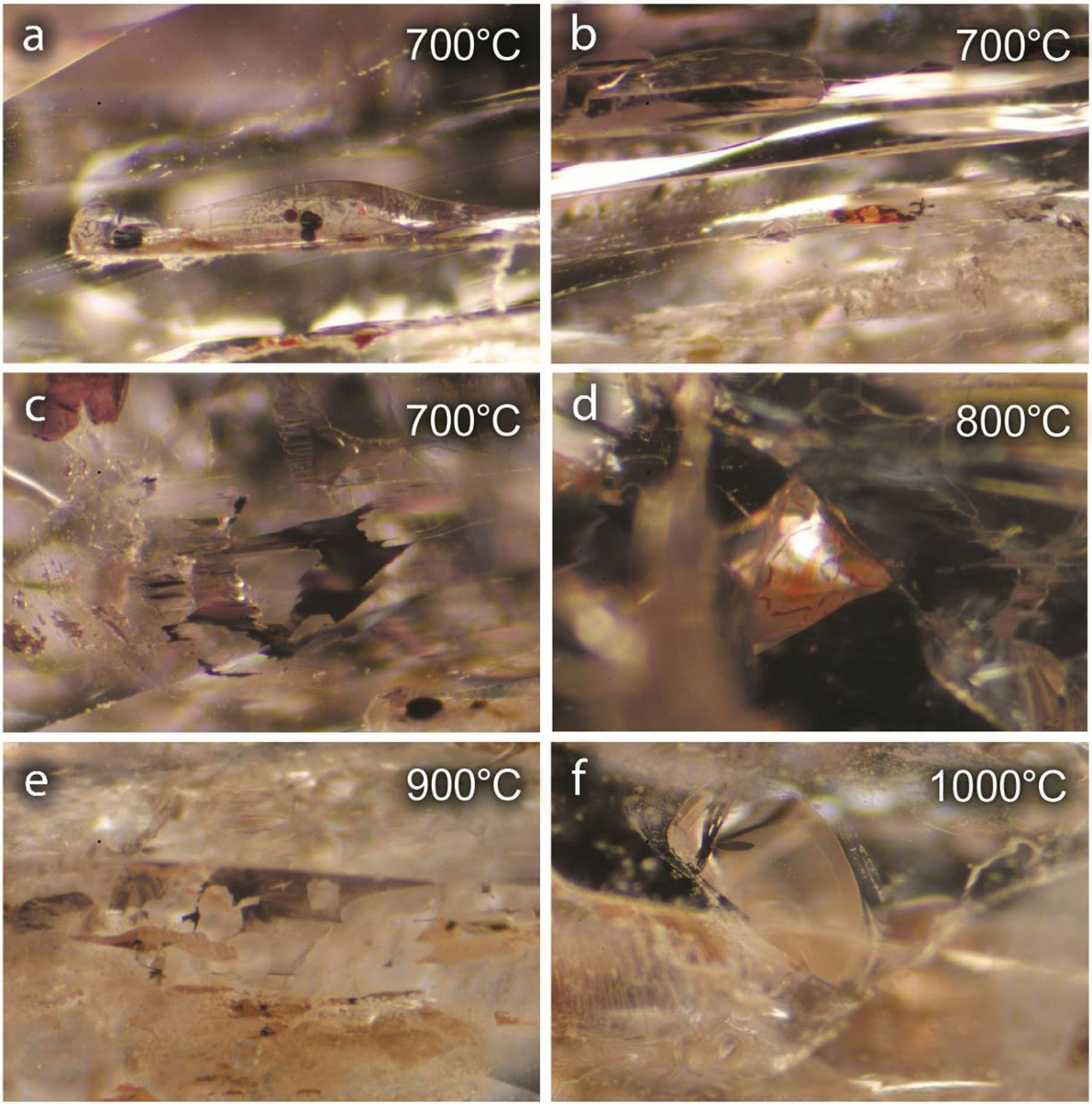

Fig. 3. Microphotographs of inclusions in OP samples heated at 700–1100 °C: a,b) brownish-yellow Fe oxide partially converted to dark reddish brown (magnification 30x); c) dried fluid inclusions (30x); d) dark reddish brown Fe oxide (20x); e,f) dried fluid inclusions (20x).

At 1100 °C, both OP and CA samples displayed pervasive cleavage propagation and transgranular microcracking, consistent with thermal stress exceeding the intrinsic fracture toughness of the topaz lattice, as observed in quartzite analogues[40]. This process is intensified by stress concentrations around inclusions and anisotropic thermal expansion, with the greatest expansion occurring along the *a*-axis and the lowest along the *c*-axis, promoting structural disruption predominantly along the basal {001} cleavage plane, which reflects the layered arrangement of tetrahedral chains and octahedral units in the topaz structure[41].

Chemical composition

Chemically, both sets of samples are very close to end-member composition based on cation content, with differences only in F and OH anions and trace elements (Table S1-S2). The CA samples are rich in F (> 1.8 apfu) and very poor in trace elements (Fe ≤ 125 ppm, and Ge ≤ 153 ppm). The OP samples contain lower F (1.4–1.5 apfu) and show elevated trace element contents (Cr up to 204 ppm, Ti up to 115 ppm, but Fe and Ge are below 64 ppm).

The OH content could not be quantified by any direct method (thermic analyses would destroy the samples, in Raman spectra, it was not possible to avoid luminescence), and in the crystal-chemical formulae of the studied sample, it was calculated as 2-F-Cl. Since the studied topazes are very close to the end-member composition,

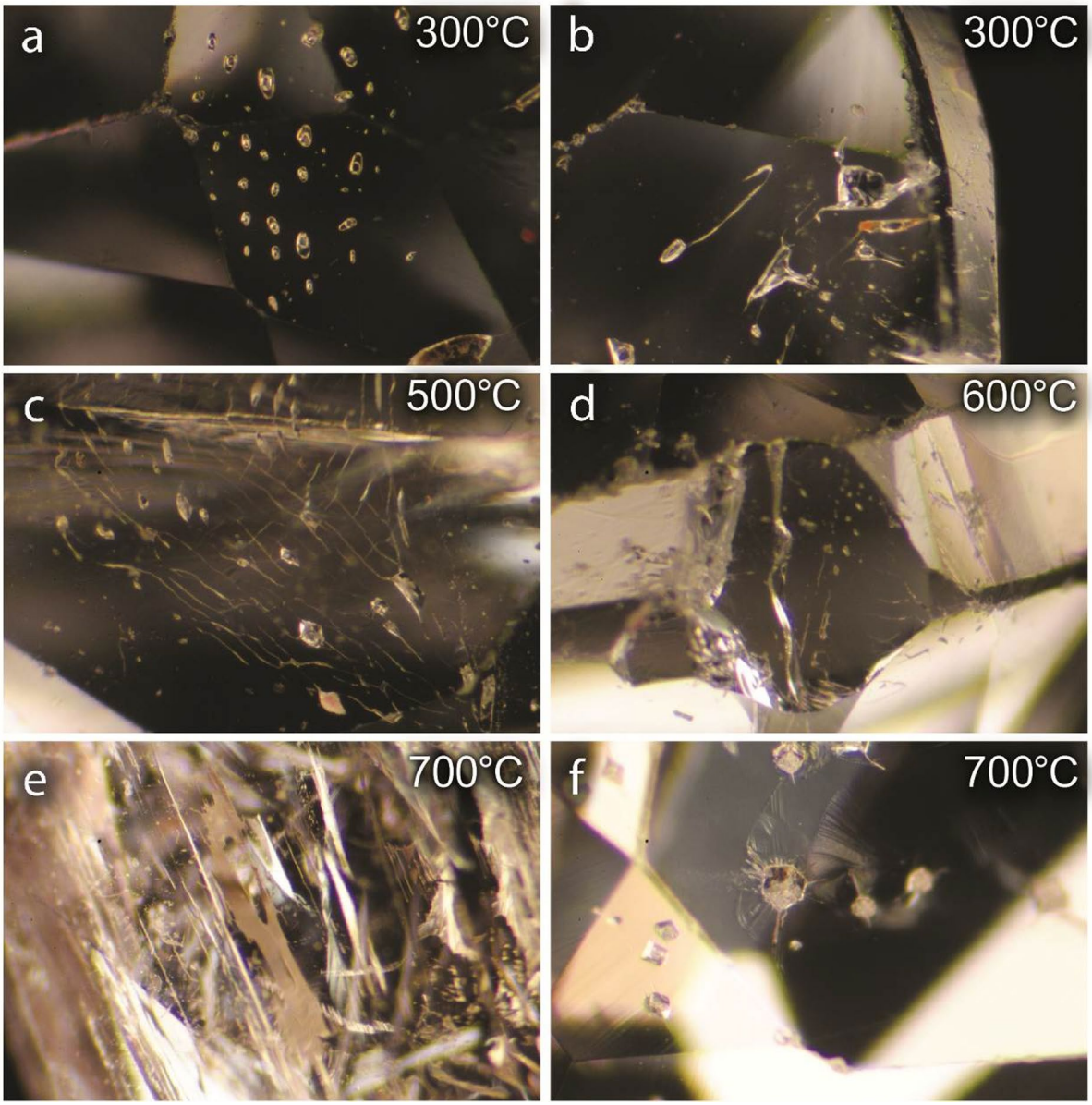

Fig. 4. Microphotographs of inclusions in CA samples heated up to 600 °C: (a) two-phase fluid inclusions (magnification 30x); (b) two-phase fluid inclusions with orange crystalised Fe oxide (30x); c, d) dried fluid inclusions network and destroyed two-phase fluid inclusions (30x); e) dried fluid inclusions (30x); f) group of crystal inclusions expanded to relieve pressure by generating a cleavage disk (30x).

it is reasonable to assume that this calculation yields correct results. No significant systematic changes in the calculated OH content, which could indicate deprotonation and release of a fluid phase during heating, were observed (Table S1-S2).

Topaz from the Ouro Preto region is known to have distinct concentrations of Ti, V, Cr, Mn, Fe, Cu, Zn, Ga, and Ge, which provide a fingerprint of imperial topaz[42]. In our studied samples of Ouro Preto imperial topaz (OP), the content of trace elements was very similar, but Mn, Fe, Cu, and Zn were very low, usually below the detection limit. In contrast, Sc is present in slightly increased content (Table S3). The blue topaz from Caraí (CA) is less variable in trace element composition, but Fe, Ge, Sc, Ti, and Ga can be considered as its fingerprint (Table S4).

The ratios of trace elements (such as Ge, V, Cr, Fe, and Ti) in topaz provide the possibility to trace its geological origin. Gem topaz is typically derived either from pegmatites, rhyolites, or hydrothermal veins[43]. In the V + Cr vs. Fe + Ti and triangular Ge vs. V + Cr vs. Fe + Ti plots (Fig. 6), the fields of topaz of different origins can be distinguished. The OP sample falls within the field of hydrothermal topaz, whereas the CA sample plots to the centre of the pegmatite and greisen field. This agrees with the genetic types of Ouro Preto and Caraí localities. To distinguish between pegmatite and greisen genetic types, other trace elements can be used; the CA sample has

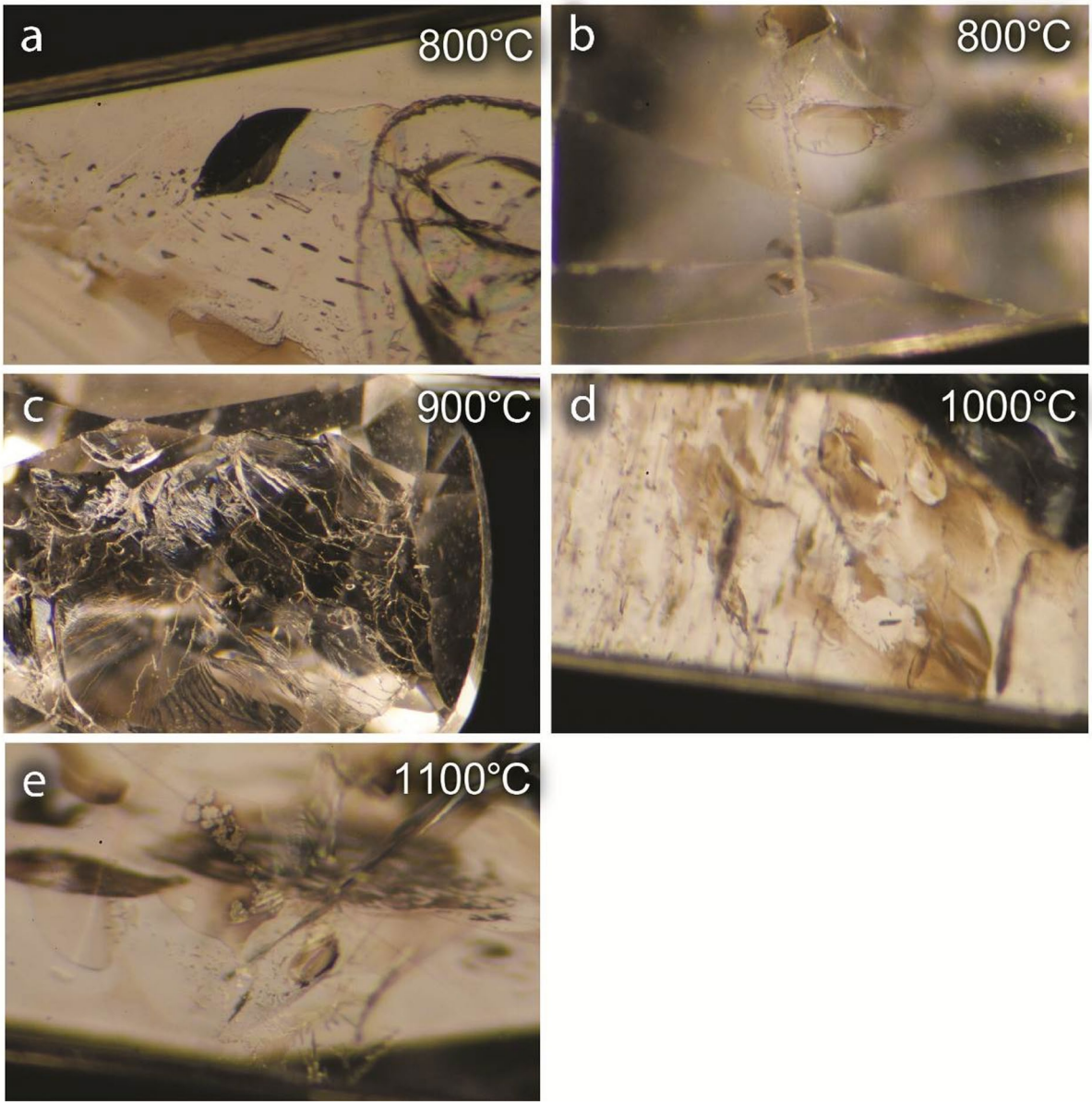

Fig. 5. Microphotographs of inclusions in CA samples heated at 800–1000 °C: (a) dried two-phase fluid inclusions (30x); (b) dried fluid inclusions with brown spots (30x); (c) a group of inclusions in expanded to relieve pressure by generating a cleavage (10x); (d) fully dried fluid inclusions (20x); (e) dried fluid inclusions with brown spots and cleavage (30x).

a very low content of Sn and W (below their respective detection limits), which are typical elements for greisen topaz[44,45]; consequently, a pegmatitic origin is more likely.

Raman spectroscopy

The main goal of Raman spectroscopy was to determine any structural changes or structural breakdown in the studied samples. Raman spectra (Tables 1 and 2) were gained from the range of 100–1200 cm^{-1} and revealed that no significant changes occurred in both sets of samples; therefore, we can assume that the topaz structure remained intact even at 1100 °C, although the visual appearance of the samples changed significantly.

The major bands for CA and OP topazes in the range of 235–290 cm^{-1} and 910–925 cm^{-1} (Fig. 7). Minor bands are located at 150–170 cm^{-1}, 330–340 cm^{-1}, 400–410 cm^{-1}, 450–465 cm^{-1}, 518–525 cm^{-1}, 1150–1188 cm^{-1}. However, it is important to note that the orientation of the measured samples (a table of faceted gemstones) was not precisely determined; therefore, the presence and intensity of each band are influenced by the random orientation of the samples. These bands are assigned according to the following sources: symmetric Si–O ring deformation (236–241 cm^{-1}[46]; various vibrational modes of SiO_4 tetrahedra (at 265–271, 283–288, 836–844 and 910–916 cm^{-1}[46,47]); stretching and bending modes of AlO_6 octahedra coupled with the bending modes of SiO_4

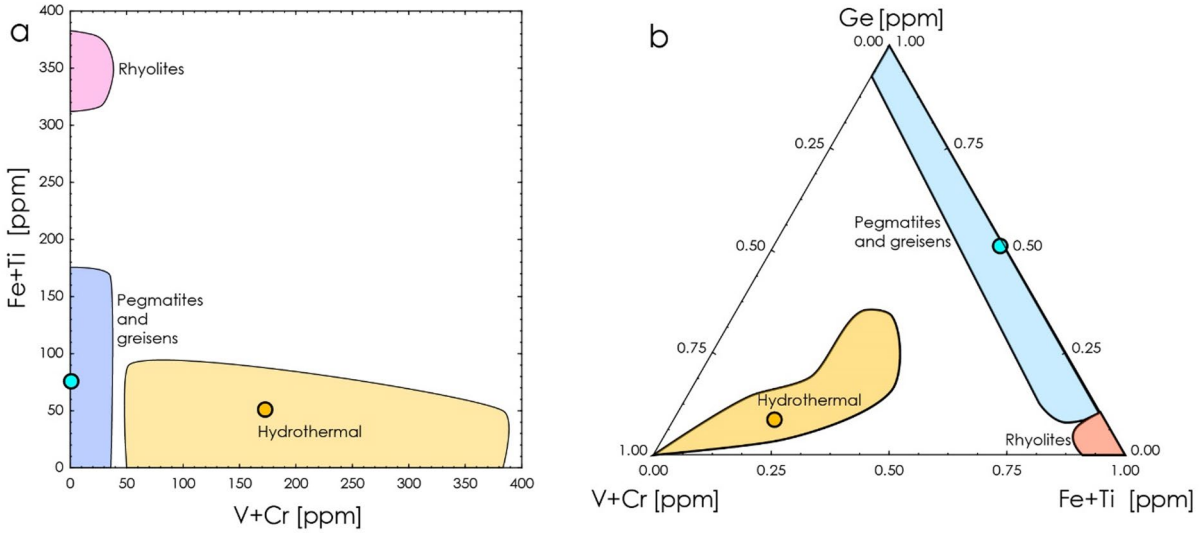

Fig. 6. Origin of samples from Ouro Preto (orange circle) and Caraí (cyan circle) based on their chemical composition (a – V + Cr vs. Fe + Ti; b – V + Cr vs. Fe + Ti vs. Ge) with fields derived from[43].

Mode	OP 300	OP 400	OP 500	OP 600	OP 700	OP 800	OP 900	OP 1000	OP 1100
-	158	158	158	157	156	157	157	157	157
ν_2 symmetric, deformation O–Si–O	241	241	236	240	240	240	240	240	236
ν_2 symmetric, deformation O–Si–O	271	271	270	270	269	270	270	270	269
ν_2 (R) symmetric, deformation O–Si–O	288	288	288	287	287	288	287	287	287
ν_4 bending Si–O	401		403	403	404	403		405	402
ν_4 bending Si–O	408	405							
ν_4 bending Si–O	458								
ν_4 bending Si–O	465	462	461	461	461	462	462	463	462
ν_4 bending Si–O	522	518	520	522	519	518	520	519	525
		525							
ν_3 antisymmetric stretching Si–O	841	841	836	840		838	839		838
			847	904		861	876		854
ν_1 symmetric stretching Si–O	927	927	926	927	928	926	926	927	925
ν_3 antisymmetric stretching $(SiO_4)^{4-}$	932	934	932		933				
ν_3 antisymmetric stretching $(SiO_4)^{4-}$		1009							1009
ν bending O–H	1154	1156	1154	1155	1157	1155	1152	1152	1159
ν bending O–H	1168	1164	1163	1179	1170	1177	1167	1169	1188

Table 1. Raman bands (in cm^{-1}) in Topaz from Ouro Preto, Brazil, and their assignment after[47].

tetrahedra (at 401–408 and 454–465 cm^{-1};[46,47]); stretching modes of Al–F (at 329–340 cm^{-1};[48]); inplane bending OH-groups (at 1152–1163 cm^{-1}[49]. Even after being observed in other studies, such as[46,48], the interpretation of bands at 519 and 642 cm^{-1} remains unclear. Bands for OH vibrations were observed in Raman spectra of only CA samples due to extremely intense luminescence of OP samples observed with all the used wavelengths of laser (532 and 633 nm). However, there is no systematic change in position or intensity of the 3650 cm^{-1} band attributed to ν_B (OH···F) according to[50]. All variations in intensity can be assigned to slight differences in OH content. Therefore, the observed behaviour of OH bands in Raman spectra is in accordance with the OH content calculated from chemical composition.

Luminescence features were observed in the Raman spectra of both samples (Fig. 8). In the OP samples, a broad luminescence bulge occurs between 650 and 800 nm, with very sharp R_1 and R_2 bands at 679 and 685 nm and a broader band at 714 nm. This luminescence can be attributed to three structurally non-equivalent Cr^{3+} centres substituting Al^{3+} in the topaz structure and forming $[CrO_4F_2]^{7-}$, $[CrO_4OH, F]^{7-}$, and $[CrO_4(OH)_2]^{7-}$

Mode	CA 300	CA 400	CA 500	CA 600	CA 700	CA 800	CA 900	CA 1000	CA 1100
-	152	152	152	152	152	152	151	152	152
ν_2 symmetric, deformation O–Si–O	237	237	237	237	237	237	237	238	237
ν_2 symmetric, deformation O–Si–O	265	265	265	265	265	265	266	266	266
ν_2 (R) symmetric, deformation O–Si–O	284	284	284	284	284	283	284	284	284
ν_4 bending Si–O	401	401	401	401	401	401	401	401	401
ν_4 bending Si–O	454	455	454	455	455	455	456	455	455
ν_4 bending Si–O				518				518	518
ν_3 antisymmetric stretching Si–O	845	845			844	852	846	845	844
ν_3 antisymmetric stretching Si–O	853	853		851	852		855	853	853
ν_1 symmetric stretching Si–O	924	923	922	924	923	924	921	923	916
ν_3 antisymmetric stretching $(SiO_4)^{4-}$	934	933	934					935	925
ν_3 antisymmetric stretching $(SiO_4)^{4-}$	1009	1006	982				980	982	982
ν_3 antisymmetric stretching $(SiO_4)^{4-}$				1004	1005	1003	1005	1008	1007
ν_3 antisymmetric stretching $(SiO_4)^{4-}$				1008	1009	1008			
ν_B (OH···F)	3650	3650	3650	3650	3650	3650	3650	3650	3650

Table 2. Raman bands (in cm^{-1}) in Topaz from Caraí, Brazil, and their assignment after[47].

complexes[51–54]. The slightly broader but still relatively sharp band at 714 nm occurring in all OP samples could also relate to the presence of the Cr^{3+} emission center[55]. These centres were described as having different thermal stability. Less stable $[CrO_4OH, F]^{7-}$, and $[CrO_4(OH)_2]^{7-}$ complexes usually diminish in the temperature range of 950–1100 °C, whereas the most stable $[CrO_4F_2]^{7-}$ centres completely decay at 1250 °C[51–54]. This could be explained by the heat-induced deprotonation of OH, which can inhibit the luminescence centre. We did not observe any change in OP spectra up to 1100 °C. This could be explained by the low OH content in the studied samples but these samples contain ca. 0.5 *apfu*. Usually, deprotonation in silicates results from oxidation of the transition element with more possible oxidation states, which can be easily oxidized, such as Mn and Fe, but in the absence of such elements, deprotonation does not occur even at the relatively high temperatures[56]. Consequently, this could explain the constancy of measured luminescence spectra.

All CA samples exhibit a luminescence bulge between 500 and 750 nm with a maximum at approximately 600 nm (Fig. 8). These samples do not contain any significant chromophores in abundance. Therefore, it would be possible to attribute it to some structural defect. However, the luminescence intensity does not change systematically; the highest intensity is observed in samples heated at 600 and 1100 °C. We assume that such high temperatures should result (at least partly) in a healing procedure, and the change in intensity would be systematic, as seen in optical spectra of the CA samples. Consequently, it is more likely that luminescence can be caused by a stable luminophore. From available elements, Mn^{2+} displays luminescence at 480–700 nm[54]. Consequently, Mn in various oxidation states could be a weak luminophore in both samples.

Optical absorption spectroscopy

The optical absorption spectra of the studied topazes were recorded between 400 and 1000 nm on samples heated at each temperature, but only those with significant differences are pictured here (Fig. 9).

The OP spectra significantly differ between samples. Those heated at 300–400 °C showed only an intense band in the blue region, centred at 415–420 nm, and a weak band in the NIR area. There is a broad area of transmission in the yellow to red region, which causes the yellowish-orange colour of topaz. However, the sample heated at temperatures of 500 °C shows a slight increase, and samples heated at 600 °C and more have a strong but broad band in the green to orange region. The absorption bands are located at 415–427 nm, 530–532 nm, 586–587 nm, and 756–760 nm. The main transmission is at ca. 700 nm in the red region and at 450–500 nm in the violet and blue region of the spectra, which enables OP samples to have an orange or pink colour. Additionally, there is a shift in the absorption edge observed towards the visible region of the spectra.

The optical spectra of OP topazes heated at 500 °C and above display a combination of absorption bands at 415–427 nm (23,500 – 24,000 cm^{-1}), 530–532 nm (18,800 cm^{-1}) to 586–587 nm (17,000 cm^{-1}). These bands can be caused by electronic spin-allowed *dd* transitions, $^4A_{2g} \leftrightarrow {}^4T_{2g}$ and $^4A_{2g} \leftrightarrow {}^4T_{1g}$, of Cr^{3+} cations in octahedrally coordinated sites[53,57–59]. However, these features are missing in the spectra of the original sample and those heated at temperatures below 500 °C. This indicates the change in oxidation state of Cr as the main chromophore in this topaz. The Cr^{4+} and Cr^{2+} centres could be generated by gamma- and X-ray irradiation[60]. However, it is possible that in gamma-irradiated ruby, the $Cr^{3+} \rightarrow Cr^{4+}$ transformation involves some crystal defects and does not result in producing Cr^{2+}[61]. One way or another, the absorption bands at 550 nm and 400 nm in irradiated ruby are close to the energy in the bands in imperial topazes[53] and can be attributed to Cr^{3+}[63]. At T > 400 °C, Cr^{4+} reduces to Cr^{3+}, the colour of imperial topazes changes to pale rose, caused by spin-allowed bands of Cr^{3+}[53].

The CA spectra exhibit strong absorption in the NIR region at 738 to 755 nm (Fig. 9). This absorption does not have any impact on the colour of the sample. In the unheated sample, the less intensive broad band is located at 634 nm, extending to the green region. This band borders the area of transmission in the cyan and blue region

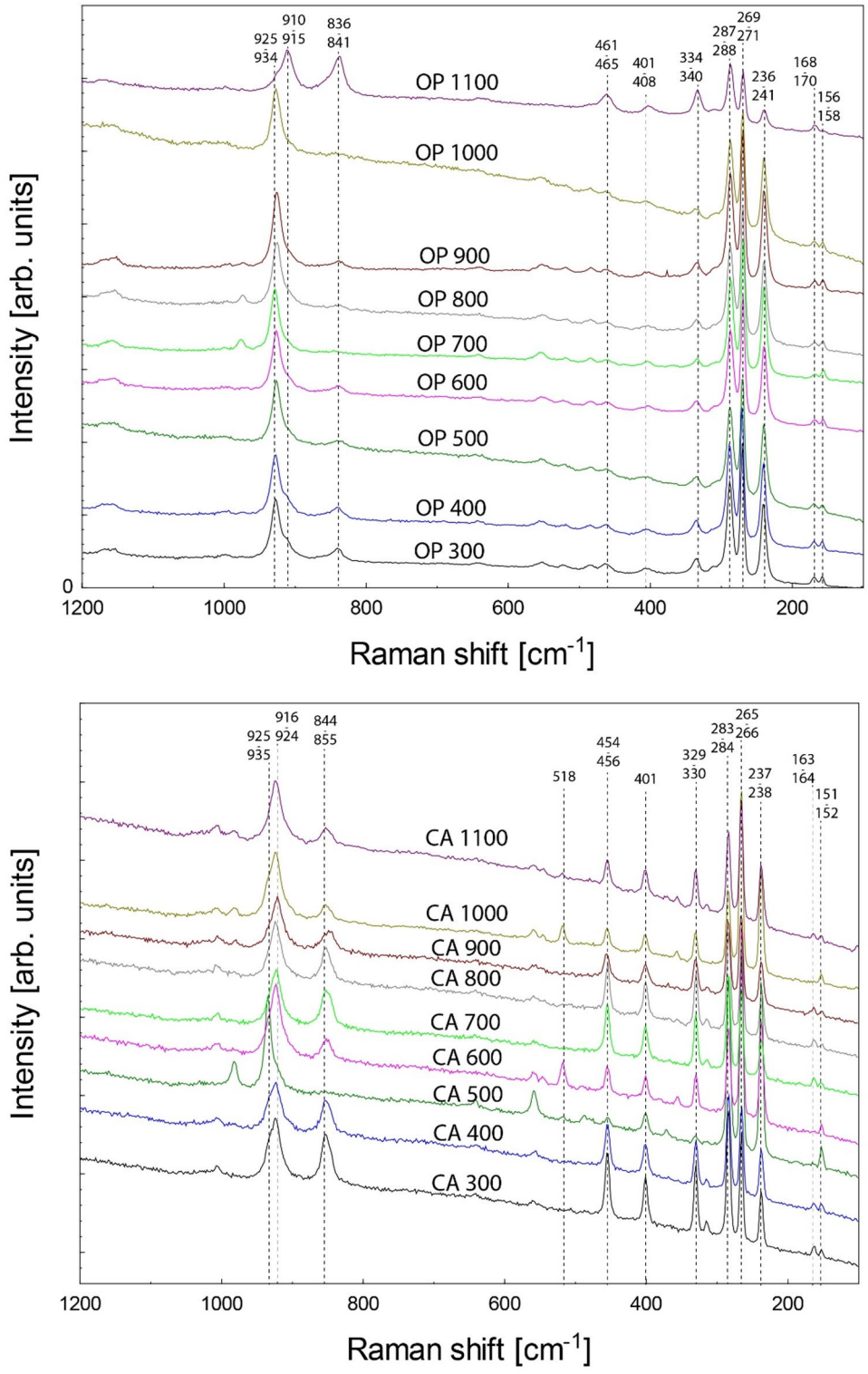

Fig. 7. Raman spectra of studied topaz samples in the region of 100–1200 cm^{-1}: OP – Ouro Preto, CA - Caraí. The most intense bands are highlighted with dashed lines.

(450–500 nm), which is responsible for the sky-blue colour of topaz. Weaker absorption bands are observed at approximately 594 to 596, 615, 634, and 664 nm in all samples, including those that have been heat-treated. However, after the heating at 300 °C and above, the transmission area in the blue to cyan region vanished, and consequently, the topaz samples lost their original blue colour.

The unheated CA spectrum is very similar to the spectra of originally colourless topaz from Minas Gerais, Brazil, which were neutron-irradiated to obtain the blue colour[33]. In their spectra, an intense, broad absorption

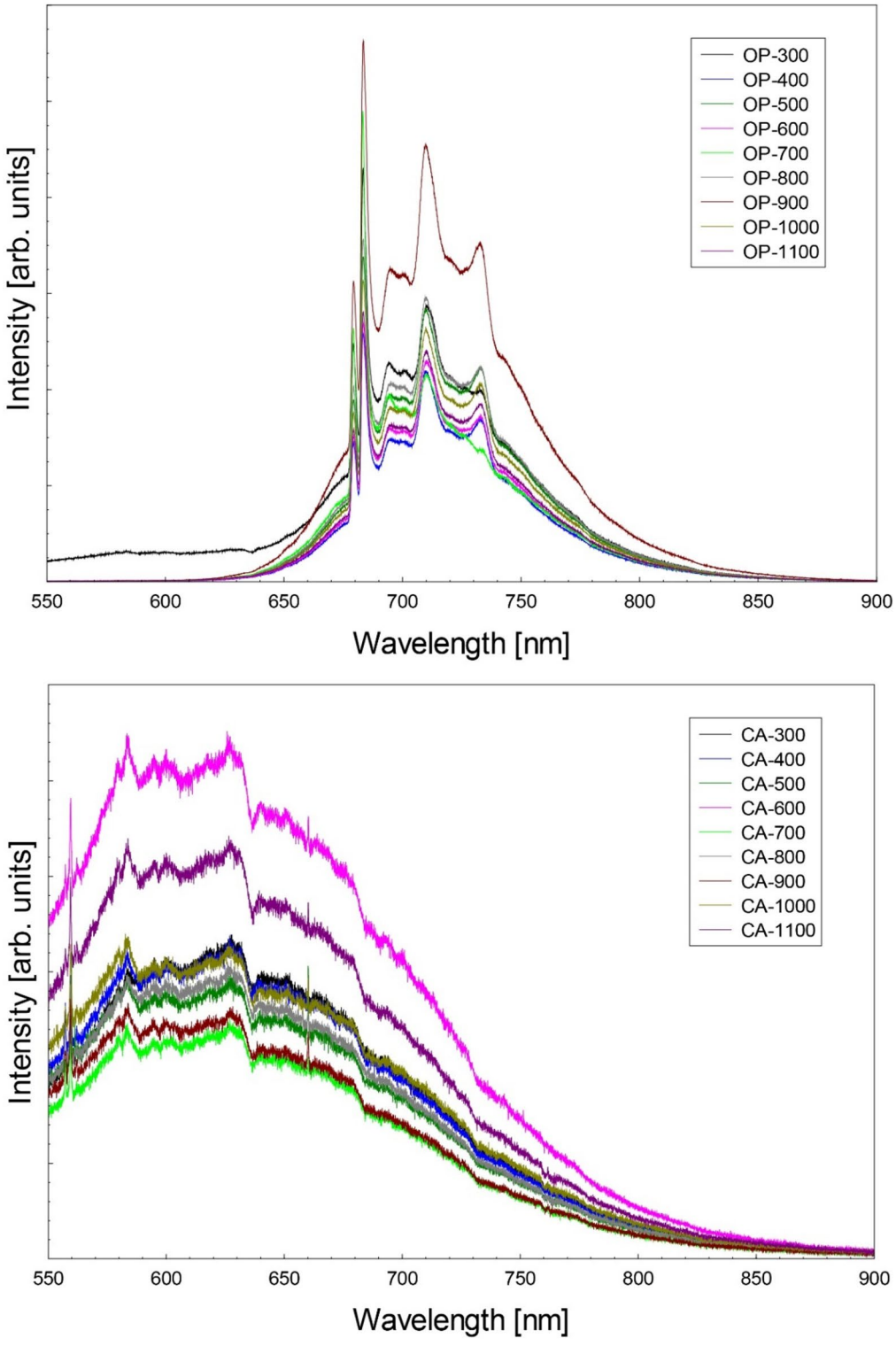

Fig. 8. Raman luminescence spectra of studied topaz samples in the region of 550–900 nm: OP – Ouro Preto, CA - Caraí.

band at about 620 nm appeared together with a less intense band at about 420 nm; the former is responsible for the blue colour. A strong increase in the absorption in the ultraviolet range and the area of transmission at approximately 475 nm were observed, resulting in a blue-coloured sample[33]. This is similar to CA samples, although a band at 420 nm is not clearly visible. The 620 nm absorption was attributed to the O^- hole centre, which occurs in neutron-irradiated blue topaz as evidenced by the electron paramagnetic resonance[62]. The O^- centre located in (8d) Wyckoff positions on fluoride sites substituted by hydroxyl molecules has superhyperfine

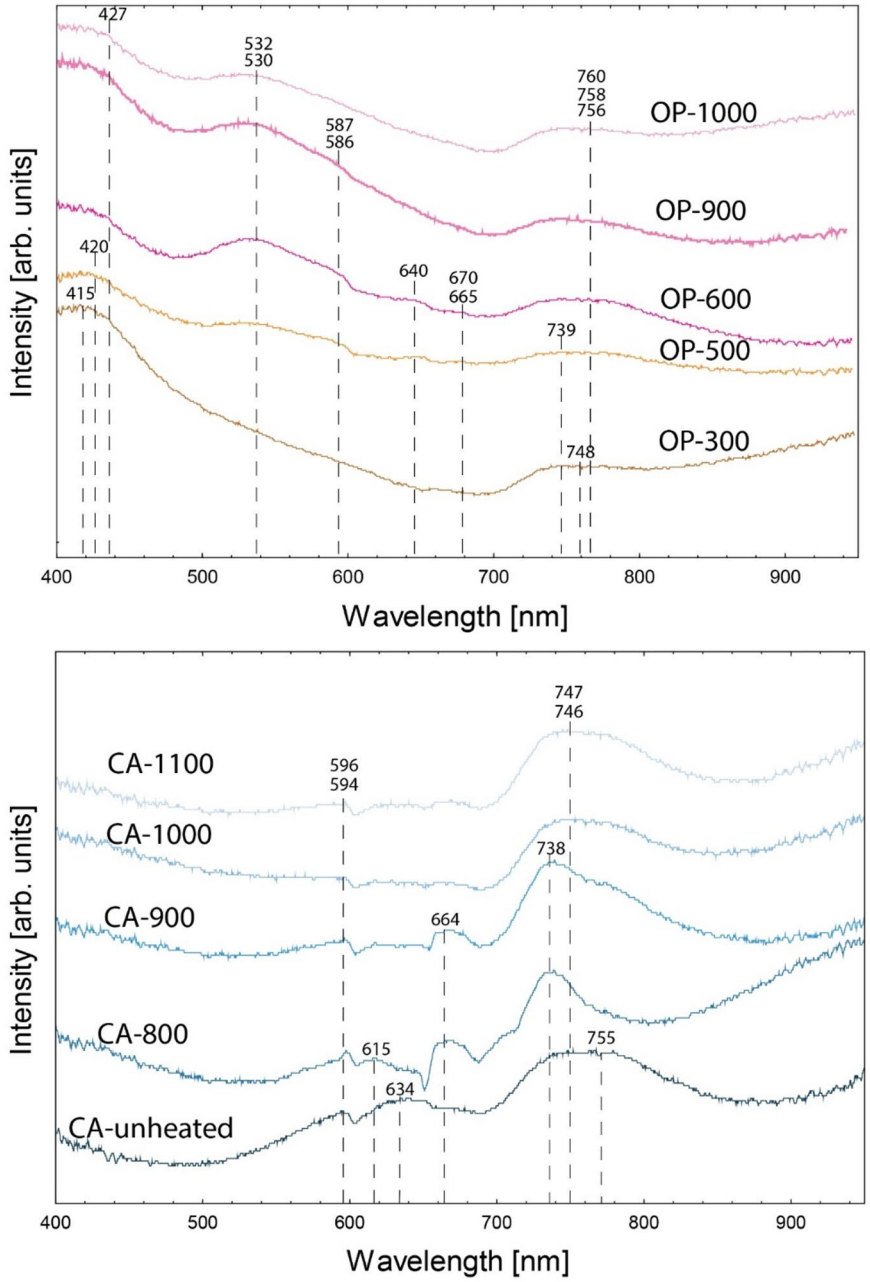

Fig. 9. Optical absorption spectra of studied topaz samples in the region of 400–950 nm: OP – Ouro Preto, CA - Caraí. The most intense bands are highlighted with dashed lines.

interactions with two equivalent Al neighbours in four magnetically inequivalent positions. The process of irradiation leads to the formation of an O^- centre by releasing a hydrogen atom from the OH group. The hydrogen atoms may form either diamagnetic H_2 molecules or be trapped at other impurities[62].

It is well-known that three irradiation sources – gamma rays, high-energy electrons, and neutrons – are used to convert the colourless stones to hues in the yellow to brown range, and the subsequent heat treatment at 220 °C for 30 min is required in most cases to turn the irradiated stones blue[36]. Compared to this, the heat treatment at 300 °C and above for several hours resulted in a diminishing of the sky-blue colour. Based on this, we can assume that heating at 220 °C for a short time was sufficient to remove colour centres responsible for yellow and brown hues, but it was unable to neutralize colour centres causing sky-blue colour. However, the heating of the CA sample at T > 300 °C resulted in the complete diminishing of the colour O^- hole centre by bonding of H back to the O anion.

Ligand field transitions and thermal stability of Cr^{3+} centres provide a contrasting mechanism of colour persistence in topaz when compared to defect-related colour centres, associated with oxygen hole states. In CA samples, the observed loss of sky-blue colour upon heating above 300 °C can be attributed to the thermal instability of oxygen hole centres (O^-), which are metastable defects generated by irradiation-induced charge

separation at hydroxyl sites. While the conventional heat treatment at 220 °C effectively removes colour centres responsible for yellow and brown hues[64], it does not neutralise the more stable O^- centres responsible for blue colouration, which arises from selective absorption of longer wavelengths in the visible spectrum[62,65]. These centres remain optically active at lower temperatures but are annihilated upon further heating due to thermally activated proton migration. The recombination of H^+ with O^- restores the O–H bond, thereby eliminating the defect-related absorption and causing complete colour loss. This behaviour differs fundamentally from the Cr^{3+}related colouration observed in OP topaz, where ligand field transitions[59] are thermally robust and persist across a wide temperature range.

Conclusions

The Ouro Preto topaz samples used in our research originally had an orange colour that remained stable up to 500 °C. At 600 °C, a pink colour with an orange tint appeared, which was most saturated at 700 °C, indicating that this is the most suitable temperature for the desired pink colour. Subsequently, its saturation rapidly decreased, and finally, at 1100 °C, it turned milky white. Between 800 °C and 1000 °C, the cracks, fissures, and clouds increased, but clarity remained translucent. It turned opaque at 1100 °C. From the spectroscopic methods, only optical absorption spectra provided evidence of a change after the heating. Samples heated at more than 600 °C developed a strong but broad band in the green to orange region.

The Caraí samples had a sky-blue colour at room temperature, their colour diminished, and it became colourless already at 300 °C and remained colourless up to 1100 °C. The clarity rapidly decreased from 700 °C to 1100 °C, accompanied by the growth of cracks and fissures and probably also partial breakdown of topaz. The CA samples showed two-phase fluid inclusions and Fe oxide inclusions. The fluid inclusions were dried and destroyed at 500 °C; samples revealed fully dry inclusions at 1100 °C. The unheated CA optical spectrum is very similar to the spectra of originally colourless topaz from Minas Gerais, Brazil, which were neutron-irradiated to obtain the blue colour[33]. It can be confirmed by the presence of bands at 620 nm; the former causes the blue colour.

The trace element composition of the studied samples is well consistent with data published[42–45] and confirms a hydrothermal origin for OP and pegmatites or greisens for CA. This agrees with the genetic types of Ouro Preto and Caraí localities.

According to our observations, we can conclude that original Ouro Preto samples with Cr in various oxidation states as the main chromophore were the most desirably enhanced to salmon-pink colour by heating at 700 °C. In contrast, the CA samples with the colour O^- hole centre lost their sky-blue colour already at 300 °C. This can be used as a potential indicator of the heat treatment of topaz declared to have an origin in these two localities. Moreover, the application of a wide variety of spectroscopic methods can be used as a cookbook for the identification of various types of gemstone treatment, not only on topazes.

Data availability

The dataset presented in the study is available on request from the corresponding author during submission or after publication.

Received: 27 August 2025; Accepted: 19 December 2025
Published online: 30 December 2025

References

1. Pichavant, M. & Manning, D. Petrogenesis of tourmaline granites and Topaz granites; the contribution of experimental data. *Phys. Earth Planet. Inter.* **35**, 31–50. https://doi.org/10.1016/0031-9201(84)90032-3 (1984).
2. Taylor, R. P. Petrological and geochemical characteristics of the pleasant ridge zinnwaldite-topaz granite, Southern new Brunswick, and comparisons with other topaz-bearing felsic rocks. *Can. Mineral.* **30**, 895–921 (1992).
3. Taylor, R. P. & Fallick, A. E. The evolution of fluorine rich felsic magmas: source dichotomy, magmatic convergence and the origins of Topaz granite. *Terra Nova*. **9**, 105–108. https://doi.org/10.1111/j.1365-3121.1997.00124.x (1997).
4. Zhang, R. Y., Liou, J. G. & Shu, J. F. Hydroxyl-rich Topaz in high-pressure and ultrahigh-pressure kyanite quartzites, with retrograde woodhouseite, from the Sulu terrane, Eastern China. *Am. Mineral.* **87**, 445–453. https://doi.org/10.2138/am-2002-0408 (2002).
5. Alberico, A., Ferrando, S., Ivaldi, G. & Ferraris, G. X-ray single-crystal structure refinement of an OH-rich Topaz from Sulu UHP terrane (Eastern China) – Structural foundation of the correlation between cell parameters and fluorine content. *Eur. J. Mineral.* **15**, 875–881. https://doi.org/10.1127/0935-1221/2003/0015-0875 (2003).
6. Holland, T. J. B., Redfern, S. A. T. & Pawley, A. R. Volume behavior of hydrous minerals at high pressure and temperature; II, compressibilities of lawsonite, zoisite, clinozoisite, and epidote. *Am. Mineral.* **81**, 341–348. https://doi.org/10.2138/am-1996-3-408 (1996).
7. Domanik, K. J. & Holloway, J. R. The stability and composition of phengitic Muscovite and associated phases from 5.5 to 11 gpa: implications for deeply subducted sediments. *Geochim. Cosmochim. Acta*. **60**, 4133–4150. https://doi.org/10.1016/S0016-7037(96)00241-4 (1996).
8. Schmidt, M. W., Finger, L. W., Angel, R. J. & Dinnebier, R. E. Synthesis, crystal structure, and phase relations of $AlSiO_3OH$, a high-pressure hydrous phase. *Am. Mineral.* **83**, 881–888. https://doi.org/10.2138/am-1998-7-820 (1998).
9. Alston, N. A. & West, J. The structure of topaz $[Al(F,OH)]_2SiO_4$. *Proc. R. Soc. Lond. Ser. A Contain. Pap. Math. Phys. Character* **121**, 358–367 (1928).
10. Pauling, L. The crystal structure of Topaz. *Proc. Natl. Acad. Sci. USA*. **14**, 603–606. https://doi.org/10.1073/pnas.14.8.603 (1928).
11. Ladell, J. Redetermination of the crystal structure of topaz: a preliminary account. *Norelco Rep.* **12**, 34–39 (1965).
12. Ribbe, P. H. & Gibbs, G. V. The crystal structure of Topaz and its relation to physical properties. *Am. Mineral.* **56**, 24–30 (1971).
13. Zemann, J., Zobetz, E., Heger, G. & Völlenkle, H. Strukturbestimmung eines OH-reichen topases. *Anzeiger Osterreichische Akademie Wissenschaften (Math.-Naturwissenschaftliche Klasse)* **116**, 145–147 (1979).
14. Parise, J. B., Cuff, C. & Moore, F. H. A neutron diffraction study of topaz: evidence for a lower symmetry. *Mineral. Mag.* **43**, 943–944. https://doi.org/10.1180/minmag.1980.043.331.21 (1980).
15. Rinne, F. X. I. I. I. Bemerkungen über optische Anomalien, Insbesondere des Brasilianer Topas. *Z. Für Kristallogr.-Crystal. Mater.* **63**, 236–246 (1926).

16. Isetti, G. & Penco, A. M. La determinazione Della posizione dell'idrogeno nell'ossidril-topazio mediante La spettrofotometria infrarossa in Luce Polarizzata. *Period Mineral.* **36**, 995–1010 (1967).
17. Ribbe, P. H. & Rosenberg, P. E. Optical and X-ray determinative methods for fluorine in Topaz. *Am. Mineral.* **56**, 1812–1821 (1971).
18. Akizuki, M., Hampar, M. S. & Zussman, J. An explanation of anomalous optical properties of Topaz. *Mineral. Mag.* **43**, 237–241. https://doi.org/10.1180/minmag.1979.043.326.05 (1979).
19. Ribbe, P. H. Topaz. In *Orthosilicates* (ed. Ribbe, P. H.) 215–230 (Mineralogical Society of America, 1982).
20. Barton, M. D. The thermodynamic properties of Topaz solid solutions and some petrologic applications. *Am. Mineral.* **67**, 956–974 (1982).
21. Barton, M. D., Haselton, H. T., Hemingway, B. S., Kleppa, O. J. & Robie, R. A. The thermodynamic properties of fluor-topaz. *Am. Mineral.* **67**, 350–355 (1982).
22. Belokoneva, E. L., Yu, Y. S. & Tsirel'son, V. G. Electron density distribution in Topaz $Al_2(SiO_4)(F,OH)_2$ as a result of accurate X-ray diffraction study. *Zh. Neorg. Khim.* **38**, 1346–1350 (1993).
23. Northrup, P. A., Leinenweber, K. & Parise, J. B. The location of H in the high-pressure synthetic $Al_2SiO_4(OH)_2$ Topaz analogue. *Am. Mineral.* **79**, 401–404 (1994).
24. Wunder, B. et al. Synthesis, stability, and properties of $Al_2SiO_4(OH)_2$: a fully hydrated analogue of Topaz. *Am. Mineral.* **78**, 285–297 (1993).
25. Wunder, B., Andrut, M. & Wirth, R. High-pressure synthesis and properties of OH-rich Topaz. *Eur. J. Mineral.* **11**, 803–813. https://doi.org/10.1127/ejm/11/5/0803 (1999).
26. Shinoda, K. & Aikawa, N. IR active orientation of OH bending mode in Topaz. *Phys. Chem. Min.* **24**, 551–554. https://doi.org/10.1007/s002690050071 (1997).
27. Bradbury, S. E. & Williams, Q. Contrasting bonding behavior of two hydroxyl-bearing metamorphic minerals under pressure: clinozoisite and Topaz. *Am. Mineral.* **88**, 1460–1470. https://doi.org/10.2138/am-2003-1010 (2003).
28. Komatsu, K., Kuribayashi, T. & Kudoh, Y. Effect of temperature and pressure on the crystal structure of topaz, $Al_2SiO_4(OH,F)_2$. *J. Mineral. Petrol. Sci.* **98**, 167–180. https://doi.org/10.2465/jmps.98.167 (2003).
29. Komatsu, K. et al. Pressure dependence of the OH-stretching mode in F-rich natural Topaz and Topaz-OH. *Am. Mineral.* **90**, 266–270. https://doi.org/10.2138/am.2005.1652 (2005).
30. Churakov, S. V. & Wunder, B. Ab-initio calculations of the proton location in topaz-OH, Al2SiO4(OH)2. *Phys. Chem. Min.* **31**, 131–141. https://doi.org/10.1007/s00269-003-0365-8 (2004).
31. Gatta, G. D., Nestola, F., Bromiley, G. D. & Loose, A. New insight into crystal chemistry of topaz: a multi-methodological study. *Am. Mineral.* **91**, 1839–1846. https://doi.org/10.2138/am.2006.2223 (2006).
32. O'Donoghue, M. *Synthetic, imitation, and Treated Gemstones* (Butterworth-Heinemann, 1997).
33. Krambrock, K. et al. Color centers in topaz: comparison between neutron and gamma irradiation. *Phys. Chem. Min.* **34**, 437–444. https://doi.org/10.1007/s00269-007-0160-z (2007).
34. Nassau, K. The effects of gamma rays on the color of beryl, smoky quartz, amethyst and Topaz. *Lapid. J.* **28**, 20–40 (1974).
35. Nassau, K. The origin of color in minerals. *Am. Mineral.* **63**, 219–229 (1978).
36. Nassau, K. Altering the color of Topaz. *Gems Gemol.* **21**, 26–34 (1985).
37. Precisvalle, N. et al. F/OH ratio in a rare fluorine-poor blue Topaz from Padre Paraíso (Minas Gerais, Brazil) to unravel Topaz's ambient of formation. *Sci. Rep.* **11**, 2666. https://doi.org/10.1038/s41598-021-82045-2 (2021).
38. Gualtieri, A. F. & Venturelli, P. In situ study of the goethite-hematite phase transformation by real time synchrotron powder diffraction. *Am. Mineral.* **84**, 895–904. https://doi.org/10.2138/am-1999-5-625 (1999).
39. Goss, C. J. The kinetics and reaction mechanism of the goethite to hematite transformation. *Mineral. Mag.* **51**, 437–451. https://doi.org/10.1180/minmag.1987.051.361.11 (1987).
40. Cathelineau, M. et al. High pressure and temperatures during the early stages of tungsten deposition at Panasqueira revealed by fluid inclusions in Topaz. *Ore Geol. Rev.* **126**, 103741. https://doi.org/10.1016/j.oregeorev.2020.103741 (2020).
41. Tennakoon, S. et al. Single crystal elasticity of natural Topaz at high-temperatures. *Sci. Rep.* **8**, 1372. https://doi.org/10.1038/s41598-017-17856-3 (2018).
42. Gauzzi, T., Graça, L. M., Lagoeiro, L. & de Mendes, C. The fingerprint of imperial Topaz from Ouro Preto region (Minas Gerais state, Brazil) based on cathodoluminescence properties and composition. *Mineral. Mag.* **82**, 943–960. https://doi.org/10.1180/minmag.2017.081.078 (2018).
43. Bassoo, R., Eames, D., Hardman, M. F., Befus, K. & Sun, Z. Topaz from Mason County, Texas. *Gems Gemol.* **59**, 414–431. https://doi.org/10.5741/GEMS.59.4.414 (2023).
44. Breiter, K., Gardenová, N. & Vaculovič, T. Topaz as an important host for ge in granites and Greisens. *Mineral. Mag.* **77**, 403–417. https://doi.org/10.1180/minmag.2013.077.4.01 (2013).
45. Agangi, A., Kamenetsky, V. S., Hofmann, A., Przybyłowicz, W. & Vladykin, N. V. Crystallisation of magmatic Topaz and implications for Nb-Ta-W mineralisation in F-rich silicic melts – The Ary-Bulak ongonite Massif. *Lithos* **202**, 317–330. https://doi.org/10.1016/j.lithos.2014.05.032 (2014).
46. Skvortsova, V., Mironova-Ulmane, N., Trinkler, L. & Chikvaidze, G. Optical properties of natural Topaz. *IOP Conf. Series: Mater. Sci. Eng.* **49**, 012051. https://doi.org/10.1088/1757-899X/49/1/012051 (2013).
47. Beny, J. M. & Piriou, B. Vibrational spectra of single-crystal Topaz. *Phys. Chem. Min.* **15**, 148–159. https://doi.org/10.1007/BF00308777 (1987).
48. Agangi, A., Gucsik, A., Nishido, H., Ninagawa, K. & Kamenetsky, V. S. Relation between cathodoluminescence and trace-element distribution of magmatic Topaz from the Ary-Bulak massif, Russia. *Mineral. Mag.* **80**, 881–899. https://doi.org/10.1180/minmag.2016.080.023 (2016).
49. Prasad, P. S. R. & Gowd, T. N. FTIR spectroscopic study of hydroxyl ions in natural Topaz. *J. Geol. Soc. India.* **61**, 202–208 (2003).
50. Watenphul, A. & Wunder, B. Temperature dependence of the OH-stretching frequencies in topaz-OH. *Phys. Chem. Min.* **37**, 65–72. https://doi.org/10.1007/s00269-009-0310-6 (2010).
51. Tarashchan, A. N. *Lyuminestsentsiya Mineralov (Luminescence of Minerals)* (Naukova Dumka, 1978).
52. Tarashchan, A. N., Taran, M. N., Rager, H. & Iwanuch, W. Luminescence spectroscopic study of Cr^{3+} in Brazilian topazes from Ouro Preto. *Phys. Chem. Min.* **32**, 679–690. https://doi.org/10.1007/s00269-005-0042-1 (2006).
53. Taran, M. N. et al. Optical spectroscopy study of variously colored gem-quality topazes from Ouro Preto, Minas Gerais, Brazil. *Phys. Chem. Min.* **30**, 546–555. https://doi.org/10.1007/s00269-003-0356-9 (2003).
54. Gaft, M., Reisfeld, R. & Panczer, G. *Modern Luminescence Spectroscopy of Minerals and Materials* (Springer, 2015). https://doi.org/10.1007/978-3-319-24765-6.
55. Gaft, M. et al. Time-resolved luminescence of Cr^{3+} in Topaz $Al_2SiO_4(OH,F)_2$. *J. Lumin.* **102–103**, 349–356. https://doi.org/10.1016/S0022-2313(02)00532-X (2003).
56. Bačík, P., Kardošová, P., Fridrichová, J., Rybnikova, O. & Škoda, R. Crystal-chemical effects of heat treatment on Cr- and V-bearing Ca-dominant green tourmalines (fluor-uvite, magnesio-lucchesiite). *Period. Mineral.* **93**, 147–164. https://doi.org/10.13133/2239-1002/18524 (2024).
57. Petrov, I., Schmetzer, K. & Eysel, H. H. Absorptionsspektren von Chrom in Topas. *Neues Neues Jahrbuch für Mineralogie Monatshefte*. **8**, 365–372 (1977).
58. Platonov, A. N., Taran, M. N. & Balitsky, V. S. *Nature of Colors of Gems (in Russian)* (Nedra, 1984).

59. Taran, M. N., Langer, K., Platonov, A. N. & Indutny, V. Optical absorption investigation of Cr^{3+} ion-bearing minerals in the temperature range 77–797 K. *Phys. Chem. Min.* **21**, 360–372. https://doi.org/10.1007/BF00203294 (1994).
60. Chao, C. C. Charge-transfer luminescence of Cr^{3+} in magnesium oxide. *J. Phys. Chem. Solids*. **32**, 2517–2528. https://doi.org/10.1016/S0022-3697(71)80098-7 (1971).
61. Zalyubovskii, I. I., Kulagin, N. A., Litvinov, L. A. & Podus, L. P. Change in the valency of chromium ions on γ-irradiation of Ruby. *Sov Phys. Solid State*. **23**, 846–849 (1981).
62. da Silva, D. N., Guedes, K. J., Pinheiro, M. V. B., Spaeth, J. M. & Krambrock, K. The microscopic structure of the oxygen–aluminium hole center in natural and neutron-irradiated blue Topaz. *Phys. Chem. Min.* **32**, 436–444. https://doi.org/10.1007/s00269-005-0018-1 (2005).
63. Sviridov, D. T., Sviridova, R. K. & Smirnov, Y. F. *Optical Spectra of Transition Metal Ions in Crystals* (Nauka, 1976).
64. Han, T. P. J., Jaque, F., Arizmendi, L., Bermudez, V. & Suchocki, A. Optical bleaching of Cr^{3+} luminescence in near-stoichiometric $LiNbO_3$ crystals codoped with MgO. *J. Lumin.* **108**, 55–58. https://doi.org/10.1016/j.jlumin.2004.01.010 (2004).
65. Chaves, A., Souza, G. P., Krambrock, K. & Caldas, L. V. E. Study of blue Topaz using different techniques of luminescence and EPR spectroscopy. *Port J. Phys.* **41**, 37–42 (2010).
66. Webster, R. *Gems: Their Sources, Descriptions and Identification* (revised by Anderson, B. W.) (Butterworths, 1984).

Acknowledgements

This work was supported by the Slovak Research and Development Agency under contract APVV-18-0065 and the VEGA Agency project VEGA-1/0189/23.

Author contributions

J.F. brought original idea, wrote the main manuscript, conducted experiments, worked on analytical methods; P.B. wrote the main manuscript, prepared figures and tables, conducted experiments, worked on analytical methods; O.R. wrote the main manuscript, worked on analytical methods; J.Š. microphotography; D.F. wrote the main manuscript, worked on analytical methods; S.F. wrote the main manuscript, worked on analytical methods; J.C. worked on analytical methods; R.Š. worked on analytical methods; T.V. worked on analytical methods. All authors reviewed the manuscript.

Funding

This work was supported by the Slovak Research and Development Agency under contract APVV-18-0065 and the VEGA Agency project VEGA-1/0189/23.

Competing interests

The authors declare no competing interests.

Additional information

Supplementary Information The online version contains supplementary material available at https://doi.org/10.1038/s41598-025-33599-y.

Correspondence and requests for materials should be addressed to J.F.